Time-resolved photoelectron spectroscopy of 4-(dimethylamino)benzethyne – an experimental and computational study

Kevin Issler, Floriane Sturm, Jens Petersen, Marco Flock, Roland Mitrić, Ingo Fischer, Lou Barreau, Lionel Poisson

PCCP

ARTICLE TYPE

Cite this: DOI: 00.0000/xxxxxxxxxx

Time-resolved photoelectron spectroscopy of 4-(dimethylamino)benzethyne - An experimental and computational study†

Kevin Issler[a], Floriane Sturm[a], Jens Petersen[a], Marco Flock[a], Roland Mitrić[a], Ingo Fischer[a], Lou Barreau[b] and Lionel Poisson[b]

Received Date
Accepted Date

DOI: 00.0000/xxxxxxxxxx

We investigated the excited-state dynamics of 4-(dimethylamino)benzethyne (4-DMABE) in a combined theoretical and experimental study using surface-hopping simulations and time-resolved ionisation experiments. The simulations predict a decay of the initially excited S_2 state into the S_1 state in only a few femtoseconds, inducing a subsequent partial twist of the dimethylamino group within $\sim$ 100 fs. This leads to drastically reduced Franck-Condon factors for the ionisation transition to the cationic ground state, thus inhibiting the effective ionisation of the molecule, which leads to a vanishing photoelectron signal on a similar timescale as observed in our time-resolved photoelectron spectra. From the phototoelectron spectra, an ionisation energy of 7.17 $\pm$ 0.02 eV was determined. The experimental decays match the theoretical predictions very well and the combination of both reveals the electronic characteristics of the molecule, namely the role of intramolecular charge transfer (ICT) states in the deactivation pathway of electronically excited 4-DMABE.

1 Introduction

Intramolecular charge transfer (ICT) is a fundamental process in which electron density is redistributed from a donor to an acceptor site within the same molecule, thus significantly changing the charge distribution with respect to the ground state.[1,2] Therefore, ICT has been a topic of remarkable interest to experimental and computational chemists for many years, considering the possible applications in organic electronics and photovoltaics.[3–7] In some organic molecules it is possible to observe a phenomenon in which an excited-state ICT leads to a second fluorescence band, as first observed by Lippert *et al.*[8,9] in the 4-(dimethylamino)benzonitrile (4-DMABN) molecule. This motivated a large amount of work on the electronic structure and character of the relevant excited states in this molecule. Numerous time-resolved experiments, ranging from transient absorption on the pico- and femtosecond time scale[10–13] to time-resolved Raman[14,15] and gas-phase spectroscopy[16,17] have been conducted in 4-DMABN. While Lippert suggested the additional band to be due to emission from the ^1L_a state that is shifted to lower energies in polar solvents, Grabowski and coworkers proposed the TICT (twisted intermolecular charge transfer) model.[2] In this model, the emissive state is stabilised by a 90° twist of the dimethylamino group with respect to the phenyl ring of the molecule in the excited electronic state. Although the charge-transfer character as well as some geometry distortion of the emissive state seem to be established, the TICT model is still debated. As an alternative, a central role of the amino inversion mode was suggested, which couples the S_1 and S_2 states.[18] Sobolewski *et al.* found a $\pi\sigma^*$ state with a bent cyano group as a minimum on the S_1 surface and proposed this state, termed "rehybridised ICT" (RICT) state, as the origin of the CT emission band.[19] Later studies proposed a sequential mechanism in which the RICT state is formed initially, followed by formation of the TICT state on a longer time scale.[11] In this context, 4-(dimethylamino)benzethyne (4-DMABE), which is depicted in Fig. 1 and isoelectronic to 4-DMABN, became an interesting reference point. Theory initially proposed a strong ten-

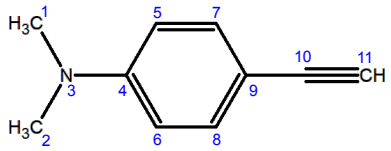

Fig. 1 Structure of the 4-(dimethylamino)benzethyne (4-DMABE) molecule with labelling of heavy atoms (blue numbers).

[a] Institute of Physical and Theoretical Chemistry, University of Würzburg, Am Hubland, D-97074 Würzburg, Germany, E-mail: ingo.fischer@uni-wuerzburg.de, roland.mitric@uni-wuerzburg.de, jens.petersen@uni-wuerzburg.de

[b] Institut des Sciences Moléculaires d'Orsay (ISMO) UMR 8214, Rue André Rivière, Bâtiment 520, Université Paris-Saclay, F-91405 Orsay Cedex, E-mail: lionel.poisson@universite-paris-saclay.fr

† Electronic Supplementary Information (ESI) available: [details of any supplementary information available should be included here]. See DOI: 10.1039/cXCP00000x/

dency for ICT,[19–21] but initial experiments did not observe dual fluorescence.[22,23] Later it was concluded from time-correlated single photon counting experiments that ICT does occur at least in strongly polar solvents, but the ICT state is not fluorescent.[24] More recently, time-resolved transient absorption spectra of both molecules in various solvents have been recorded[11,25] and the photophysics was characterised computationally employing multireference perturbation theory.[26] Based on these investigations, it was proposed that the photodynamics in polar solution is characterised by two parallel paths, in which either a locally excited (LE) state which is structurally similar to the ground state, or, alternatively, the bent $\pi\sigma^*$ state, are populated. In 4-DMABN, formation of the TICT state proceeds as a second step, while the respective pathway is blocked for energetic reasons in 4-DMABE.

For a systematic comparison of experiments with high-level theory it seems necessary to study isolated molecules in order to separate the intrinsic molecular dynamics from solvent motion. Experimentally, 4-DMABN itself in the gas phase has been investigated with high resolution spectroscopy[27,28] as well as femtosecond time-resolved spectroscopy,[17] and the initial steps of the photodynamics have been simulated using the surface-hopping dynamics approach.[29,30] In contrast, no studies have been reported for 4-DMABE that would permit the comparison of computations with gas phase data.

We therefore initiated a combined experimental and computational study of 4-DMABE in the gas phase to better understand the photophysics of the isolated molecule. To this end, we employed surface-hopping dynamics simulations[31] in combination with time-resolved photoelectron spectroscopy (TRPES).[32] It has been shown that this approach makes it possible to disentangle contributions from different electronic states to the ionisation signal and thus allows one to follow nonradiative intramolecular dynamics in real time.[33–38] TRPES has been also successfully employed to study a few related isolated molecules exhibiting ICT,[39] indicating its applicability.

2 Methods

The picosecond time-resolved experiments have been conducted in Würzburg with a setup depicted in Fig. S1 in the electronic supporting information (ESI) and described in detail recently.[40,41] It consists of a 10 Hz Nd:YLF laser and an optical parametric amplifier. The laser system has a time-resolution of 4-5 ps and a bandwidth of around 20-25 cm^{-1}.

The femtosecond time-resolved experiments were carried out at the ATTOlab laser platform at LIDYL,[42] Université Paris-Saclay, using a setup combining velocity map imaging (VMI) and time-of-flight mass spectrometry (TOF-MS) that has been described before[36], and is also given in Fig. S2 in the ESI. 4-DMABE, commercially obtained from Sigma-Aldrich, was held at room temperature, seeded in 1.1 bar of helium and expanded into a differentially-pumped vacuum chamber by a 100 μm nozzle. The source chamber was operated at a pressure of 3.5×10^{-4} mbar. The resulting jet then passed a 1 mm skimmer, expanding into the detection chamber held at a pressure of 1.8×10^{-6} mbar. Around 15 cm into the detection chamber, the pump and probe laser beams crossed the molecular beam in the center of the ion optics. The ion and electron spectrometers were oriented perpendicular to the laser/jet plane. By applying different voltage gradients, VMI of the electrons/ions were collected on one detector. The VMI detector consists of two microchannel plates and a phosphor screen, with a sCMOS camera imaging the spatial distribution of the charged particles. In addition, time-of-flight mass spectra were recorded on a dual-stage microchannel plate detector in the opposite direction, but are not discussed in the present manuscript.

The tripled fundamental of a Ti:Sa laser (1 kHz, 23 fs) operated between 265 and 272 nm was used as the pump pulse (43 μJ at most). For the probe pulse, either the fundamental of the Ti:Sa laser (794 nm, 1.18 mJ at most) or its second harmonic (397 nm, $\approx$ 200 μJ at most) was employed. At least two photons at 794 nm or one photon at 397 nm are necessary to ionise 4-DMABE from its excited states. Both laser beams enter the detection chamber from the same side with a small crossing angle and are softly focused (f=750 mm lens) in the interaction region with the molecular beam. The distances to the focal points were chosen to minimise one-colour ionisation. The probe pulse was delayed with respect to the pump pulse using a computer-controlled stepper motor. The time intervals between the points varied between 10 fs close to the pump-probe overlap and up to 167 fs far away from it, the points being measured randomly. Each delay trace consists of at least 4 individual delay scans. The photoelectron spectra were integrated over 3750 laser shots for each point. The polarisation of the pump laser was rotated for each point between parallel and perpendicular with respect to the probe laser.

For the theoretical description of the vertical electronic excitation energies several computational methods were compared as summarised in Table 1. Specifically, the algebraic diagrammatic construction through second order (ADC(2))[43–45] method in its spin-component scaling (SCS) variant[46,47] together with the aug-cc-pVDZ[48,49] and d-aug-cc-pVDZ[48–50] basis sets was used in the framework of the Turbomole program package[51] . Furthermore, employing the Gaussian16 program package,[52] time-dependent density functional theory (TDDFT) was employed using the long-range corrected CAM-B3LYP[53] and ωB97XD[54] functionals and the aug-cc-pVDZ and 6-311++G**[55,56] basis sets, as well as the equation-of-motion coupled cluster approach with single and double excitations (EOM-CCSD)[57–60] with the 6-311++G** basis set. The excited states of 4-DMABE are well described within the ADC(2)/aug-cc-pVDZ level of theory, which therefore was subsequently employed for the surface hopping simulations. It needs to be mentioned, though, that the ground state is treated at the second-order perturbation theory (MP2) level within this approach, which does not provide reasonably accurate ionisation energies. These are adequately described within the (EOM-)CCSD and (TD-)DFT methodologies, which, however, give rise to systematically too high excitation energies.

In addition to the vertical excitation energies, geometry optimizations in the excited state have been performed for several isomers employing the TDDFT/ωB97XD/aug-cc-pVDZ level of theory in the frame of the QChem program package.[61] The nature of the stationary points has been examined by calculating the vibrational frequencies and normal modes. Vibronic Franck-Condon

Table 1 Vertical excitation energies and ionisation energies in eV, oscillator strengths [in brackets] and state characters (in brackets) for 4-DMABE.

Energy	ADC(2)		EOM-CCSD	CAM-B3LYP		ωB97XD		Experiment
	aug-cc-pVDZ	daug-cc-pVDZ	aug-cc-pVDZ	aug-cc-pVDZ	6-311++G**	aug-cc-pVDZ	6-311++G**	(adiabatic)
S_1	4.31 [0.02] ($\pi\pi^*$)	4.31	4.50 [0.02]	4.55 [0.04]	4.62 [0.04]	4.55 [0.04]	4.62 [0.04]	3.95
S_2	4.61 [0.39] ($\pi\pi^*$)	4.58	4.74 [0.17]	4.67 [0.26]	4.73 [0.30]	4.78 [0.57]	4.82 [0.58]	4.34
S_3	4.89 [0.22] (s-Ryd)	4.83	5.09 [0.43]	4.81 [0.37]	4.88 [0.33]	5.03 [0.07]	5.11 [0.07]	
IE_{ad}	8.27		6.97	7.01	7.05	7.00	7.03	7.17
IE_{vert}	10.02		7.33	7.16	7.21	7.15	7.20	

progressions have been calculated based on the obtained normal modes using the ezFCF program.[62,63]

For the quantum-classical dynamics simulations, the surface-hopping methodology as proposed by Tully[31] was utilised, coupled to quantum-chemical calculations at the ADC(2)/aug-cc-pVDZ level of theory using the Turbomole program package. From those results scalar non-adiabatic couplings and electronic transition dipole moments were evaluated using a procedure explained in detail in Refs.[33,64,65]. The classical nuclear dynamics was simulated by integration of Newton's equations of motion using the velocity Verlet algorithm[66] with an integration time step of 0.2 fs. Considering the ground and the three energetically lowest excited states, the electronic population dynamics was determined along the classical trajectories by solving the time-dependent Schrödinger equation including the non-adiabatic couplings between all electronic states. This yields time-dependent electronic state populations from which surface-hopping probabilities are evaluated. The ensemble of 100 initial conditions was sampled from a harmonic Wigner distribution function for the vibrational ground state and the dynamics was started with the population in the second excited electronic state, simulating the relaxation after initial vertical excitation.

3 Results and Discussion

In a first series of experiments one-color REMPI spectra were recorded with a ps-laser in the energy region covering the two lowest electronically excited states, as depicted in Fig. 2a. Consistent with the theoretical predictions, a lower-lying weak band and a higher-lying strong one are present, which can be identified with the L_b (S_1) and L_a (S_2) states of $\pi\pi^*$ character[19] found at the ground state geometry (cf. Table 1). For an interpretation of the vibrational structure, the possible excited state isomers have to be discussed first. Four distinct isomers in the lowest excited state have been described in the literature[26]: the locally excited (LE) state whose geometry only slightly differs from that of the ground state, the fully twisted TICT and the partially twisted pTICT state, as well as the $\pi\sigma^*$ or RICT state characterized by a bent acetylene group. We have optimized these states at the TDDFT/ωB97XD/aug-cc-pVDZ level of theory and illustrate their geometries in the ESI, Fig. S3, while the excitation energies and transition dipole moments are summarised in Table 2. In our calculations, the specific twisting angles for the TICT and pTICT structures are 86° or 18°, respectively, while the CCC bending angle of the $\pi\sigma^*$ state amounts to 127°. It should be noted that the stationary points representing the above-mentioned states all lie on the S_1 electronic potential energy surface, although they may correlate with higher-lying states at the ground state geometry.

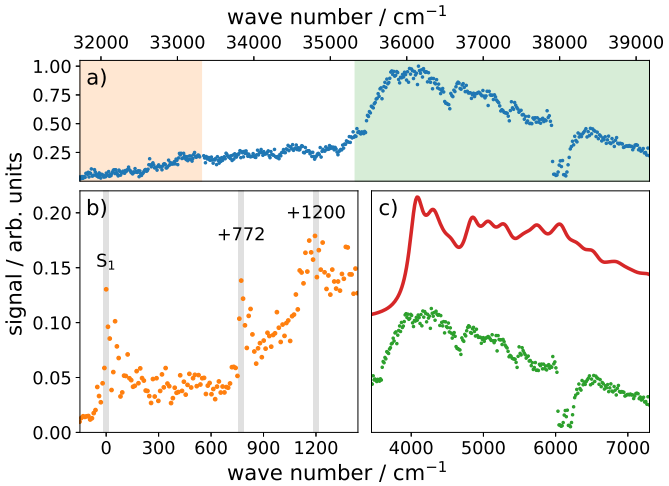

Fig. 2 a) Experimental one-color REMPI spectrum of 4-DMABE obtained using a ps-laser. The displayed energy ranges of b) and c) are indicated in orange and green, respectively. b) Lower-energy region of the recorded [1+1'] REMPI spectrum with λ_{probe} = 351 nm. Three bands marked in grey represent the S_1 origin at 31854 cm^{-1} and two vibrationally excited states. c) Higher-energy region of the one-color REMPI spectrum (green) and simulated Franck-Condon progression at T=200 K for vibronic transitions from the S_0 to the LE state (red), shifted +930 cm^{-1} to match the experimental progression. The individual transition lines (not shown) have been broadened by a Lorentzian width of 100 cm^{-1}. The spectrum has been obtained at the TDDFT/ωB97XD/aug-cc-pVDZ level of theory. The spectra in b) and c) are shifted so that the S_1 origin is at 0 cm^{-1}.

In particular, the LE state correlates with the bright L_a (S_2) state. Based on the theoretical data, we identify the weak experimental band with the pTICT and the strong one with the LE state. The low-energy weak band has been additionally investigated in a [1+1'] experiment, which provides a better signal-to-noise ratio. For ionisation, the 3^{rd} harmonic of Nd:YLF laser at 351 nm has been employed. The data are presented in Fig. 2b and allow the identification of several vibronic bands. A band with moderate intensity appears at 31854 cm^{-1}, corresponding to 313.9 nm or 3.95 eV and is assigned to the vibronic origin (marked as S_1 in 2b). A further band at +772 cm^{-1} could be assigned to a phenyl deformation mode computed at 809 cm^{-1} in the pTICT state. In ps-time-resolved experiments both the origin transition and the band at +772 cm^{-1} exhibit a ns-lifetime (see ESI, Fig. S4b and c), confirming that the state giving rise to the weak band is long lived. A further recognizable band appears around +1200 cm^{-1}. Theoretically, there are a lot of different vibrational modes to be found in this energy region, so given the broadness of the peak it is not possible to assign this band to a specific mode.

Table 2 Adiabatic (ΔE_{ad}) and vibronic 0-0 (ΔE_{00}) transition energies as well as squared transition dipole moments ($|\mu_{01}|^2$) for transitions from the ground state to several stationary points of the S_1 state and the cation, obtained at the TDDFT/ωB97XD/aug-cc-pVDZ level of theory.

Structure	ΔE_{ad}/eV	ΔE_{00}/eV	$\lvert\mu_{01}\rvert^2/e^2a_0^2$
LE [a]	4.542	4.340	5.606
pTICT	4.366	4.199	0.355
$\pi\sigma^*$	3.734	3.700	0.045
TICT	4.308	4.149	0.009
Cation D_0	7.000	7.014	

[a] the LE structure exhibits 1 imaginary vibrational frequency

To further investigate the first excited state, we also recorded photoelectron spectra via the two lower identified bands in Fig. 2b (S_1 origin, +772 cm^{-1}), presented on the left-hand side of Fig. 3. Ionisation with a probe wavelength of 351 nm via the S_1 origin leads to electrons with an electron kinetic energy (EKE) of 0.31 eV. When this value is subtracted from the total photon energy of 7.48 eV, we deduce an adiabatic ionisation energy IE_{ad} = 7.17 eV. This is in good agreement with the value of 6.97 eV, computed at the CCSD/aug-cc-pVDZ level of theory as well as with the values obtained using DFT (cf. Table 1). The two spectra exhibit a similar shape, which indicates that transitions preserving the respective vibrational quantum number are dominant. This indicates a molecular structure that changes only slightly upon ionisation, which is in accordance with the theoretically obtained ground state geometries for the neutral and cationic molecule. The right-hand side of Fig. 3 shows the spectra as a function of vibrational excess energy in the ion. A band at +900 cm^{-1} is visible, which suggests a vibrational energy increase of $\sim$ 130 cm^{-1} upon ionisation. The spectrum recorded via the excited vibrational state is broadened due to transitions into additional cationic vibrational states.

The strong band seen in the REMPI spectrum is identified with the transition to the LE state. The simulated vibrationally broadened absorption spectrum is presented together with the experimental data in Fig. 2c . The calculated 0-0 transition at 35004 cm^{-1} (4.34 eV) at the ωB97XD/aug-cc-pVDZ level of theory matches well the first experimental peak around 36000 cm^{-1}. The characteristic bands of the experimental progression are also reproduced reasonably, as can be seen in Fig. 2c. The observed dip in signal strength between 37930 cm^{-1} and 38130 cm^{-1} is due to a drop in laser intensity within this small energy region and does not impact the surrounding data. Compared to the situation for the weak band, the time-delay traces recorded after excitation in the bright band change markedly (see ESI Fig. S4d and e). They show two components, a fast one that is below the time-resolution of the setup and a second one with a long time constant in the ns region. Hence, contrary to the S_1 state, the dynamics in the S_2 state cannot be fully resolved with the ps-setup. Therefore, in order to unveil the ultrafast processes taking place after excitation into the S_2 state, a combined approach of surface-hopping dynamics and fs-TRPES was employed.

Accordingly, we initiated our nonadiabatic dynamics simulations in the L_a (S_2) state, and also included the next higher state, which is situated at 4.89 eV in the ground state geometry and can be classified as an s-type Rydberg state. With changing molecular

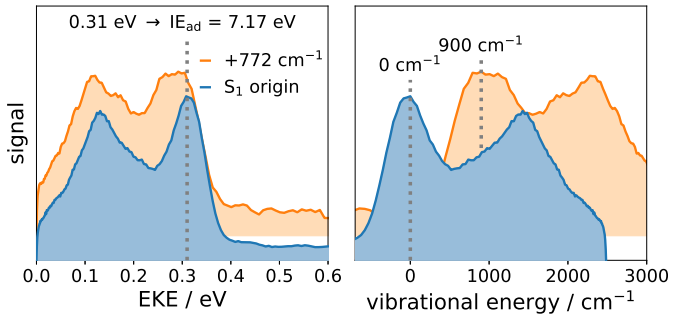

Fig. 3 [1+1'] photoelectron spectra recorded via the origin and one vibrational band indicated in Fig. 2. From the EKE an IE of 7.17 eV is derived.

geometry, the character of the states may change, though. In particular, it should be noticed that with our choice of the number of excited states also all of the states given in Table 2 are covered, as these all belong to the S_1 potential energy surface, albeit at different geometries. From the population dynamics depicted in Fig. 4a it is clear that very rapidly about 70% of the population flows into the S_1 state, while only a small fraction resides in the higher states for the simulation time of 250 fs. With regard to the time-dependent ionisation energies, most part of the trajectories should be photo-ionisable by using 397 nm photons in the entire time range. However, as detailed below, in the experiment the time-resolved photoelectron signal quickly disappears within about 100 fs after initial excitation. As a reason, we propose the geometrical deformations of the molecules taking place in the S_1 state.

To this end, we have classified the structures occurring during the dynamics simulations according to their similarity to the excited state isomers discussed before. As a prerequisite, we define the following angles (in the expressions below, $\mathbf{e}_{i,j}$ denotes a unit vector pointing in the direction of the line connecting atoms i and j according to the numbering given in Fig. 1):

$$\alpha = \arccos(\mathbf{e}_{3,4}\cdot(\mathbf{e}_{1,3}\times\mathbf{e}_{2,3})) - \frac{\pi}{2} \quad (1)$$

$$\beta = \arccos(\mathbf{e}_{9,10}\cdot\mathbf{e}_{10,11}) \quad (2)$$

$$\gamma = \arccos(\mathbf{e}_{1,2}\cdot\mathbf{e}_{5,6}), \quad (3)$$

where α can be interpreted as a measure for pyramidalisation at the amino group nitrogen atom, β describes the CCC bending at the acetylene group and γ measures the torsion of the dimethylamino moiety with respect to the phenyl ring. For the assignment to any of the 4-DMABE isomers, we require $\alpha < 45°$. Furthermore, for the bent structure of the $\pi\sigma^*$ state, $\beta > 20°$ and $\gamma < 15°$, while for the ground state (GS) and the twisted structures, $\beta < 20°$ must be fulfilled. A GS-like structure is then characterised by $\gamma \leq 15°$, pTICT by $15° < \gamma \leq 45°$ and TICT by $\gamma > 45°$.

The resulting time-dependent structural populations are presented in Fig. 4b and make clear that although the excited state remains S_1 in most trajectories during the entire simulation time, the geometry deviates from the original ground state structure

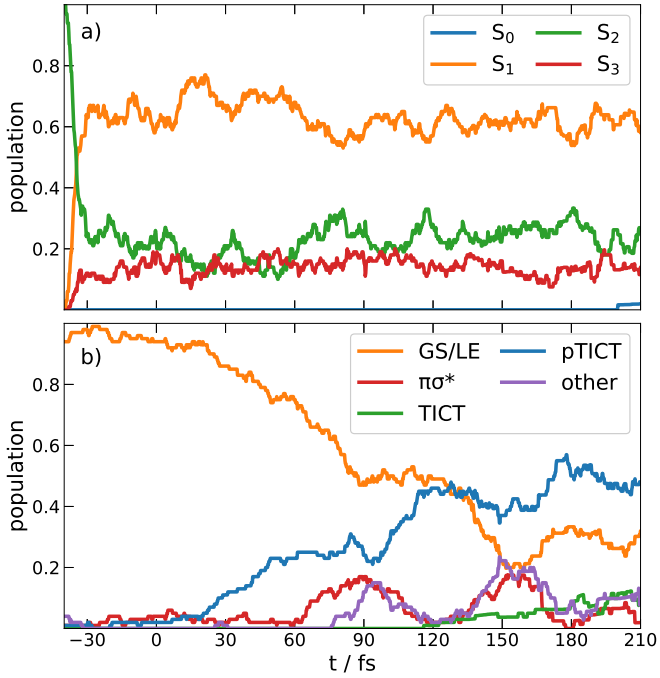

Fig. 4 a) Time-dependent electronic state populations of 4-DMABE during the ADC(2) surface-hopping simulation initiated in the S_2 state. b) Time-dependent population of characteristic 4-DMABE conformers during the ADC(2) surface-hopping simulation. Both populations are averaged over 100 trajectories. The time axis was shifted to match the experimental pump-probe delay.

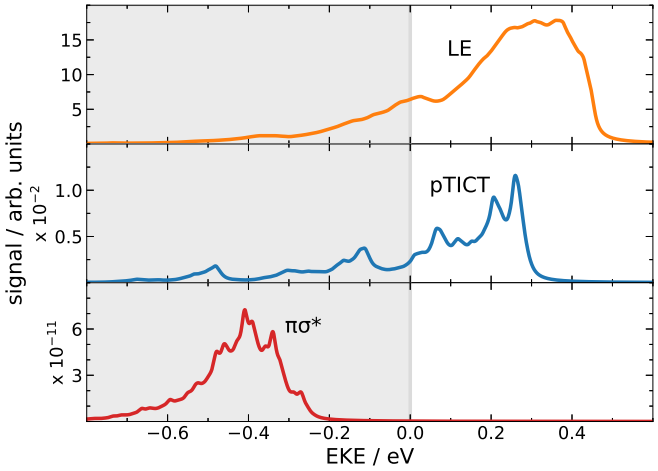

Fig. 5 Vibronic Franck-Condon spectra for the ionisation transitions between the indicated neutral 4-DMABE S_1 state conformations and the cationic ground state. As the horizontal axis, the photoelectron kinetic energy (EKE) for a 3.12 eV (397 nm) probe step has been chosen. The individual transition lines (not shown) have been broadened by a Lorentzian width of 0.01 eV. Areas shaded in grey correspond to formally negative kinetic energies, thus, intensities in these regions are not observable. Notice the drastically different ranges of the y-axis for the three spectra.

very quickly, in about 50% of the cases becoming pTICT-like, while other structures also occur to a smaller extent. This has profound implications on the Franck-Condon factors and thus the signal intensities for the ionisation transitions.

To make the point more quantitative, we have computed the Franck-Condon spectra for the photoionisation to the cationic ground state starting from the LE, pTICT and $\pi\sigma^*$ excited state structures, as depicted in Fig. 5. As the energy axis, the photoelectron kinetic energy obtained when using a single 397 nm probe photon was chosen in order to meet the experimental conditions. In this way, parts of the spectrum appear at negative energies (emphasised by grey background), corresponding to the fact that the ionisation energy in this region is higher than the photon energy, and thus no intensity would be experimentally observed. Two significant observations can be made from the figure: (i) Only molecules at the LE or pTICT, but not at the $\pi\sigma^*$ geometry can be ionised with one photon, (ii) the signal intensity for ionisation from the LE geometry is more than three orders of magnitude higher as compared to the pTICT geometry. This clearly indicates that a structural change from the LE (which itself is close to the ground state geometry) to the pTICT geometry should be accompanied by a drastic decrease of ionisation signal intensity.

In the following, the connection between these theoretical findings with the results of femtosecond time-resolved experiments will be made. The experiments were conducted using time-resolved photoelectron spectroscopy (TRPES). Pump pulses with a central wavelength between 265 nm and 272 nm were employed, but no differences were observed between them. For ionisation, probe wavelengths of 397 nm and 794 nm were employed.

A TRPES recorded using 397 nm probe is provided in Fig. 6. A structureless band is visible, peaking at low EKE. The cutoff at around 0.5 eV is in excellent agreement with a [1+1'] ionisation process, considering the 7.66 eV total photon energy and the ionisation energy of 7.17 eV, as determined above. The signal decays rapidly to zero and exhibits a half-life of about 50 fs. This confirms a fast dynamics on the excited state potential energy surface. As discussed above, the theoretical findings suggest that on a time scale of several hundred fs, the system stays in the S_1 state (cf Fig. 4a). The decisive point, however, is the structural dynamics of the molecule. While the ionisation threshold hardly changes upon slight twisting of the initially planar structures (cf. Fig. 5), the formation of pTICT-like geometries quickly leads away from the Franck-Condon region, thus reducing the ionisation probability to the cationic ground state due to smaller Franck-Condon factors. This is clearly discernible from the comparison of the decaying signal for pump-probe delays between -30 and 220 fs (Fig. 6b) with the time-dependent amount of ground-state-like geometries in the dynamics simulation (Fig. 6c), which show a very similar temporal behaviour.

In a second set of experiments, the probe wavelength was shifted to 794 nm. At least two probe photons are now required to reach the ionisation threshold. Due to the higher laser power available, such multiphoton processes are straightforward. As visible in Fig. 7, the appearance of the spectrum changes conspicuously. The 2D map now shows two components, one at low EKEs between 0 and 0.5 eV, labelled A, with maximal intensity around $t = 0$ ps, and a second one, labelled B, that is slightly shifted in time and maintains considerable intensity at EKE < 1.2 eV at all delay times. The experimental data show a strong rota-

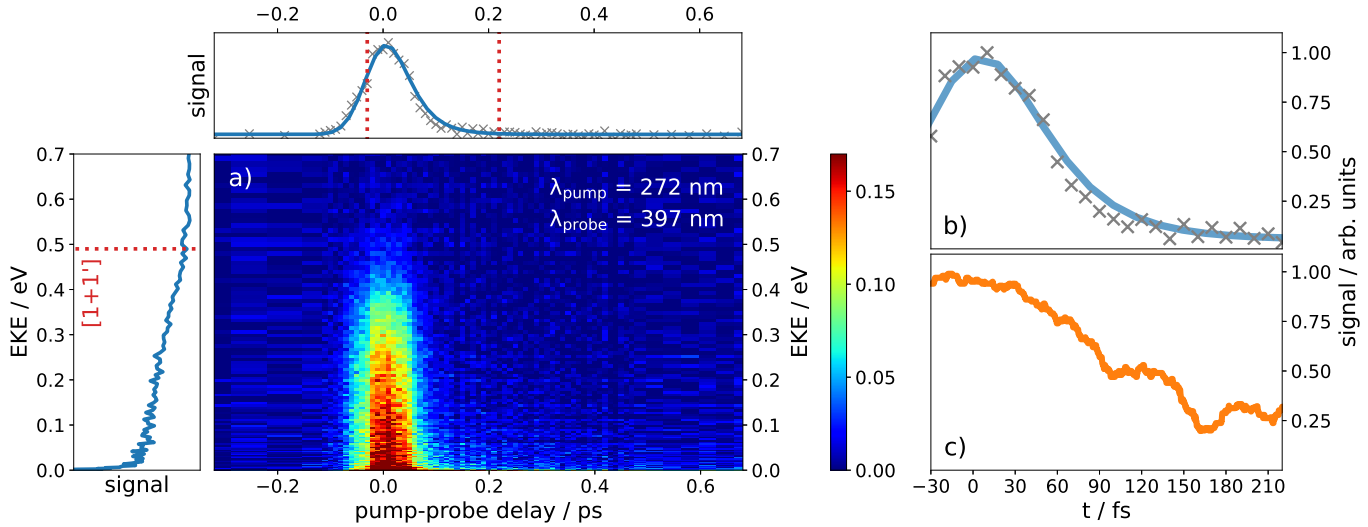

Fig. 6 a) Time-resolved photoelectron spectrum of 4-DMABE, recorded with 397 nm probe. The data were corrected for rotational anisotropy (cf. ESI, Fig. S7). Left panel: Time-integrated photoelectron spectrum. The maximum energy for 1-photon probe ionisation is indicated by the red dotted line. Upper panel: Total energy-integrated signal. A rapid decay is observed with a half-life of about 50 fs. b) Enlarged view of the decaying signal intensity. c) Simulated time-dependent population of molecular structures close to the ground state minimum geometry. Notice that this figure is reprinted as Fig. S5 in the ESI employing a perceptually uniform, sequential colormap for the 2D-plot (panel a) in order to ease interpretation in greyscale.

tional anisotropy (cf. ESI, Fig. S8) that was corrected in the Fig. 7 by taking the appropriate ratio from parallel and orthogonal polarization[67] ($I_{\parallel} + 2I_{\perp}$). From the photoelectron spectrum at the left-hand side of the figure we conclude that this component is due to a three-photon ionisation in the probe step. Component A shows a rapid decay to about 2/3 of its maximal intensity, again with a half-life of $\sim$ 50 fs similar to the observations for the 397 nm experiments. In contrast to the experiments at 397 nm probe, it does not decay to zero but retains a considerable, almost time-independent offset that is similar to the observations for component B. The latter increases with a delay also on the order of 50 fs and stays at constant level at least for about a ps. Its appearance can be understood as a stepwise process through intermediate states, enabling an ionisation pathway that was energetically possible but previously not accessible due to the molecule moving out of the Franck-Condon region. Note that the $\pi\sigma^*$ geometry can be ionized by three 794 nm photons, but the computed signal intensity is several orders of magnitude smaller, so we do not expect this process to be relevant.

Therefore, the theoretical and experimental data suggest a sequential model, in which the initially excited S_2 state first decays to the S_1 state on a time scale faster than the experimental time resolution. This state can be ionised by one photon of 397 nm (or two of 794 nm). On a time scale of 50 fs, the corresponding electron signal vanishes completely in the case of 397 nm probe wavelength, while a weak, nearly constant offset remains with 794 nm probe, which is attributed to three-photon ionisation. The presence of two ultrafast time scales finds its parallels in experimental time-resolved ionisation data of the 4-DMABN molecule where two sub-ps time constants could be identified.[16] This behaviour seems to be caused by the geometrical change of the molecules to a slightly twisted (pTICT) structure on the S_1 potential energy surface, for which the one-photon ionisation probability is strongly diminished. These findings are quite similar to previous ADC(2)-surface-hopping results of Kochman *et al.*[29,30] on the 4-DMABN molecule in the gas phase where a sub-10-fs internal conversion from the initial S_2 to the S_1 state is followed by structural deformation to a slightly twisted geometry. Notice, that the final conclusion of the aforementioned work is the absence of TICT formation in the gas phase, although in Ref.[29] a fair amount of full twisting was observed. This was attributed to the energetic underestimation of the TICT structure within the ADC(2) method, in contrast to its spin-opposite scaled (SOS) variant which was employed in Ref.[30]. In our simulations, we used the more general spin-component scaling (SCS) ADC(2) method which is however very similar to SOS-ADC(2).[46,47] Therefore, also in our simulations no appreciable TICT formation occurred. This is in agreement with experimental data where for 4-DMABE neither dual fluorescence[24] nor transient absorption features that could be attributed to a TICT state[11] were observed. Interestingly, we only find a very small contribution of structures with bent acetylene group (the $\pi\sigma^*$ or "rehybridized" intramolecular CT structure, RICT, of Sobolewski and Domcke[19–21]) which was inferred to play a key role in the photophysics of 4-DMABE by Lee et al.[11] and Segarra-Martí and Coto.[26] One reason for that may be that the $\pi\sigma^*$ structure is strongly polarised and thus much less stable in the gas phase than in polar solvents, similar to the TICT structure. Besides that, for 4-DMABN very recently the assignment of those features in the measured transient absorption (TA) spectra that were previously attributed to the $\pi\sigma^*$ state has been challenged by Kochman et al.,[68] who have simulated the TA spectrum based on surface-hopping dynamics and have found the aforementioned TA signal to be due to excited state absorption of the LE state. A similar situation might also exist in the case of

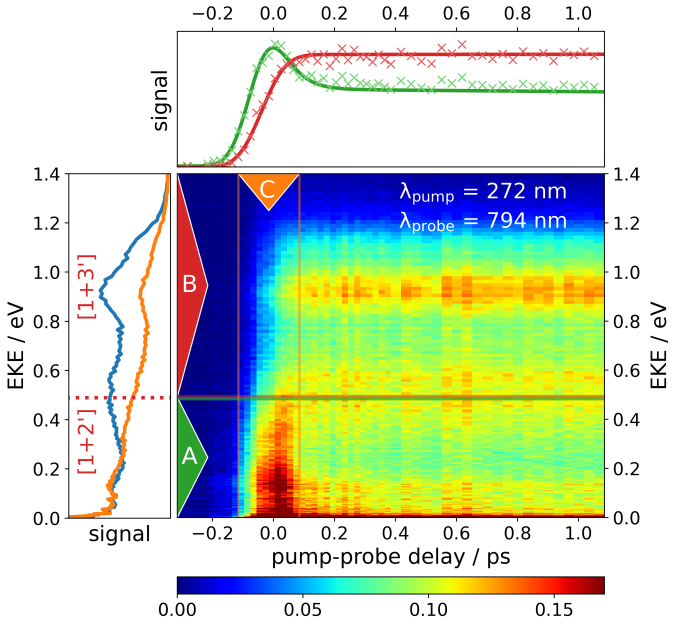

Fig. 7 Time-resolved photoelectron spectrum of 4-DMABE photoexcited at 272 nm, recorded with 794 nm probe. The rotational anisotropy was removed (see text and ESI, Fig. S8). Left panel: Total time-integrated photoelectron spectrum (blue) and short-time spectrum (orange) integrated over the time span indicated by C in the 2D plot. Upper panel: Total signal intensity integrated over the energy regions A (green) and B (red) indicated in the 2D plot. For each set of data points the maximum signal was set to 1. The rapid decay of the initially excited state gives rise to an electronic state that remains excited for $>$ 10 ps. The photoelectron spectrum shows that it is associated with electrons of high kinetic energy that originate from a [1+3'] ionisation. Notice that this figure is reprinted as Fig. S6 in the ESI employing a perceptually uniform, sequential colormap for the 2D-plot (middle panel) in order to ease interpretation in greyscale.

4-DMABE.

4 Conclusions

We conducted a joint theoretical and experimental study on the excited state dynamics of 4-(dimethylamino)benzethyne (4-DMABE). The first excited state (S_1) was observed to be stable with respect to deactivation on a ns-time scale and therefore investigated using photoelectron spectroscopy (PES), pumping various (vibrational) states observed in REMPI experiments conducted beforehand. An adiabatic IE of 7.17 eV was determined for 4-DMABE. The second excited state (S_2) was observed to deactivate on a timescale unresolvable with a picosecond setup. Therefore this ultrafast photorelaxation dynamics of 4-DMABE after optical excitation at 272 nm was investigated using time-resolved photoelectron spectroscopy (TRPES) on a fs-timescale. Theoretically, starting in the second excited state after vertical excitation we simulated the relaxation of the system using the surface-hopping approach, revealing a fast deactivation in less than 10 fs into the first excited state, which is stable with respect to electronic relaxation on the observed timescale. The initial deactivation is followed by a change in geometry to a structure with a partially twisted dimethylamino group out of the molecular plane (pTICT) on the timescale of $\sim$ 100 fs. Twisting of the amino group is accompanied by a drastically decreasing transition dipole moment for the ionisation process due to diminishing Franck-Condon factors. Hence the structural change of the molecule can directly be linked to the photoelectron intensity, which is in perfect agreement with our TRPES experiments showing a matching temporal intensity evolution. In our TRPES using a probe wavelength of 794 nm, a quasi-constant non-zero intensity was also observed. Although the underlying complex multiphoton process is theoretically not accessible, we observed that in our simulations 4-DMABE is energetically ionisable at all times from its excited states. This suggests the involvement of intermediate states in the multiphoton ionisation, making the process more feasible in comparison to single-photon ionisation, where the small Franck-Condon factors inhibit effective ionisation.

Overall we were able to bring to light the deactivation pathway after excitation and resolve the role of twisted structures in the characteristic ionisation properties of 4-DMABE. While a prolonged dispute was found in the literature whether after excitation the molecular structure remains planar or changes to a perpendicularly twisted geometry in 4-DMABE and related molecules, in this case we found that the truth may lie between the two extremes.

Conflicts of interest

There are no conflicts to declare.

Acknowledgements

The work was funded by the Deutsche Forschungsgemeinschaft, contract FI575/16-1 and MI1236/6-1. The research leading to these results has received funding from LASERLAB-EUROPE (grant agreement no. 871124, European Union's Horizon 2020 research and innovation programme). F.S. thanks the Rosa-Luxemburg-Foundation for a PhD fellowship. The authors kindly thank Jean-François Hergott, Fabien Lepetit and Olivier Tcherbakoff for setting up and maintaining the ATTOLab laser. LP acknowledges ANR11-EQPX0005-ATTOLAB.

Notes and references

1 *Intramolecular Charge Transfer*, John Wiley & Sons, Ltd, 2018, ch. 1, pp. 1–27.
2 Z. R. Grabowski, K. Rotkiewicz and W. Rettig, *Chem. Rev.*, 2003, **103**, 3899–4032.
3 W. Rettig, *Angew. Chem. Int. Ed.*, 1986, **25**, 971–988.
4 B. O'Regan and M. Grätzel, *Nature*, 1991, **353**, 737 – 740.
5 J. M. Szarko, B. S. Rolczynski, S. J. Lou, T. Xu, J. Strzalka, T. J. Marks, L. Yu and L. X. Chen, *Adv. Funct. Mater.*, 2014, **24**, 10–26.
6 W. Li, Y. Pan, L. Yao, H. Liu, S. Zhang, C. Wang, F. Shen, P. Lu, B. Yang and Y. Ma, *Adv. Opt. Mater.*, 2014, **2**, 892–901.
7 S. Sasaki, G. P. C. Drummen and G.-i. Konishi, *J. Mater. Chem. C*, 2016, **4**, 2731–2743.
8 E. Lippert, W. Lüder, F. Moll, W. Nägele, H. Boos, H. Prigge and I. Seibold-Blankenstein, *Angew. Chem.*, 1961, **73**, 695–706.

9 E. Lippert, W. Lüder and H. Boos, *Advances in Molecular Spectroscopy*, Pergamon, 1962, pp. 443–457.

10 C. Chudoba, A. Kummrow, J. Dreyer, J. Stenger, E. Nibbering, T. Elsaesser and K. Zachariasse, *Chem. Phys. Lett.*, 1999, **309**, 357–363.

11 J.-K. Lee, T. Fujiwara, W. G. Kofron, M. Z. Zgierski and E. C. Lim, *J. Chem. Phys.*, 2008, **128**, 164512.

12 S. Druzhinin, N. Ernsting, S. Kovalenko, L. Lustres, T. Senyushkina and K. Zachariasse, *J. Phys. Chem. A*, 2006, **110**, 2955–2969.

13 T. Fujiwara, M. Z. Zgierski and E. C. Lim, *Phys. Chem. Chem. Phys.*, 2011, **13**, 6779–6783.

14 J. M. Rhinehart, R. D. Mehlenbacher and D. McCamant, *J. Phys. Chem. B*, 2010, **114**, 14646–14656.

15 S. K. Sahoo, S. Umapathy and A. W. Parker, *Appl. Spectrosc.*, 2011, **65**, 1087–1115.

16 W. Fuß, K. K. Pushpa, W. Rettig, W. E. Schmid and S. A. Trushin, *Photochem. Photobiol. Sci.*, 2002, **1**, 255–262.

17 S. Trushin, T. Yatsuhashi, W. Fuß and W. Schmid, *Chem. Phys. Lett.*, 2003, **376**, 282–291.

18 K. Zachariasse, T. Vonderhaar, A. Hebecker, U. Leinhos and W. Kuhnle, *Pure Appl. Chem.*, 1993, **65**, 1745–1750.

19 A. Sobolewski and W. Domcke, *Chem. Phys. Lett.*, 1996, **259**, 119–127.

20 A. Sobolewski and W. Domcke, *J. Photochem. Photobiol. A*, 1997, **105**, 325–328.

21 A. Sobolewski, W. Sudholt and W. Domcke, *J. Phys. Chem. A*, 1998, **102**, 2716–2722.

22 K. A. Zachariasse, M. Grobys and E. Tauer, *Chem. Phys. Lett.*, 1997, **274**, 372 – 382.

23 K. A. Zachariasse, T. Yoshihara and S. I. Druzhinin, *J. Phys. Chem. A*, 2002, **106**, 6325–6333.

24 N. Chattopadhyay, C. Serpa, M. Pereira, J. de Melo, L. Arnaut and S. Formosinho, *J. Phys. Chem. A*, 2001, **105**, 10025–10030.

25 T. Fujiwara, J.-K. Lee, M. Z. Zgierski and E. C. Lim, *Phys. Chem. Chem. Phys.*, 2009, **11**, 2475–2479.

26 J. Segarra-Martí and P. B. Coto, *Phys. Chem. Chem. Phys.*, 2014, **16**, 25642–25648.

27 A. Nikolaev, G. Myszkiewicz, G. Berden, W. Meerts, J. Pfanstiel and D. Pratt, *J. Chem. Phys.*, 2005, **122**, 084309.

28 A. J. Fleisher, R. G. Bird, D. P. Zaleski, B. H. Pate and D. W. Pratt, *J. Phys. Chem. B*, 2013, **117**, 4231–4240.

29 M. A. Kochman, A. Tajti, C. A. Morrison and R. J. D. Miller, *J. Chem. Theory Comput.*, 2015, **11**, 1118–1128.

30 M. A. Kochman and B. Durbeej, *J. Phys. Chem. A*, 2020, **124**, 2193–2206.

31 J. C. Tully, *J. Chem. Phys.*, 1990, **93**, 1061–1071.

32 M. S. Schuurman and V. Blanchet, *Phys. Chem. Chem. Phys.*, 2022, **24**, 20012–20024.

33 R. Mitrić, U. Werner and V. Bonačić-Koutecký, *J. Chem. Phys.*, 2008, **129**, 164118.

34 A. Humeniuk, M. Wohlgemuth, T. Suzuki and R. Mitric, *J. Chem. Phys.*, 2013, **139**, 134104/1–134104/9.

35 K. Issler, A. Röder, F. Hirsch, L. Poisson, I. Fischer, R. Mitrić and J. Petersen, *Faraday Discuss.*, 2018, **212**, 83–100.

36 A. Röder, J. Petersen, K. Issler, I. Fischer, R. Mitrić and L. Poisson, *J. Phys. Chem. A*, 2019, **123**, 10643–10662.

37 S. Karashima, A. Humeniuk, R. Uenishi, T. Horio, M. Kanno, T. Ohta, J. Nishitani, R. Mitrić and T. Suzuki, *J. Am. Chem. Soc.*, 2021, **143**, 8034–8045.

38 S. Karashima, X. Miao, A. Kanayama, Y.-i. Yamamoto, J. Nishitani, N. Kavka, R. Mitric and T. Suzuki, *J. Am. Chem. Soc.*, 2023, **145**, 3283–3288.

39 S. Aloïse, Z. Pawlowska, C. Ruckebusch, M. Sliwa, J. Dubois, O. Poizat, G. Buntinx, A. Perrier, F. Maurel, P. Jacques, J.-P. Malval, L. Poisson, G. Piani and J. Abe, *Phys. Chem. Chem. Phys.*, 2012, **14**, 1945–1956.

40 M. Flock, M.-P. Herbert and I. Fischer, *Chem. Phys.*, 2018, **515**, 744–749.

41 M. Flock, L. Bosse, D. Kaiser, B. Engels and I. Fischer, *Phys. Chem. Chem. Phys.*, 2019, **21**, 13157–13164.

42 A. Golinelli, X. Chen, B. Bussière, E. Gontier, P.-M. Paul, O. Tcherbakoff, P. D'Oliveira and J.-F. Hergott, *Opt. Express*, 2019, **27**, 13624–13636.

43 J. Schirmer, *Phys. Rev. A*, 1982, **26**, 2395–2416.

44 A. B. Trofimov and J. Schirmer, *J. Phys. B*, 1995, **28**, 2299–2324.

45 C. Hättig, *Response Theory and Molecular Properties (A Tribute to Jan Linderberg and Poul Jørgensen)*, Academic Press, 2005, vol. 50, pp. 37–60.

46 S. Grimme, *J. Chem. Phys.*, 2003, **118**, 9095–9102.

47 A. Hellweg, S. Grün and C. Hättig, *Phys. Chem. Chem. Phys.*, 2008, **10**, 1159–1169.

48 T. H. Dunning, *J. Chem. Phys.*, 1989, **90**, 1007–1023.

49 R. A. Kendall, T. H. Dunning and R. J. Harrison, *J. Chem. Phys.*, 1992, **96**, 6796–6806.

50 D. E. Woon and T. H. Dunning, *J. Chem. Phys.*, 1994, **100**, 2975–2988.

51 *TURBOMOLE V7.0 2015, a development of University of Karlsruhe and Forschungszentrum Karlsruhe GmbH, 1989-2007, TURBOMOLE GmbH, since 2007; available from* `http://www.turbomole.com`.

52 M. J. Frisch, G. W. Trucks, H. B. Schlegel, G. E. Scuseria, M. A. Robb, J. R. Cheeseman, G. Scalmani, V. Barone, G. A. Petersson, H. Nakatsuji, X. Li, M. Caricato, A. V. Marenich, J. Bloino, B. G. Janesko, R. Gomperts, B. Mennucci, H. P. Hratchian, J. V. Ortiz, A. F. Izmaylov, J. L. Sonnenberg, D. Williams-Young, F. Ding, F. Lipparini, F. Egidi, J. Goings, B. Peng, A. Petrone, T. Henderson, D. Ranasinghe, V. G. Zakrzewski, J. Gao, N. Rega, G. Zheng, W. Liang, M. Hada, M. Ehara, K. Toyota, R. Fukuda, J. Hasegawa, M. Ishida, T. Nakajima, Y. Honda, O. Kitao, H. Nakai, T. Vreven, K. Throssell, J. A. Montgomery, Jr., J. E. Peralta, F. Ogliaro, M. J. Bearpark, J. J. Heyd, E. N. Brothers, K. N. Kudin, V. N. Staroverov, T. A. Keith, R. Kobayashi, J. Normand, K. Raghavachari, A. P. Rendell, J. C. Burant, S. S. Iyengar, J. Tomasi, M. Cossi, J. M. Millam, M. Klene, C. Adamo, R. Cammi, J. W. Ochterski, R. L.

Martin, K. Morokuma, O. Farkas, J. B. Foresman and D. J. Fox, *Gaussian~16 Revision A.03*, 2016, Gaussian Inc. Wallingford CT.

53 T. Yanai, D. P. Tew and N. C. Handy, *Chem. Phys. Lett.*, 2004, **393**, 51–57.

54 J.-D. Chai and M. Head-Gordon, *Phys. Chem. Chem. Phys.*, 2008, **10**, 6615–6620.

55 T. Clark, J. Chandrasekhar, G. W. Spitznagel and P. V. R. Schleyer, *J. Comput. Chem.*, 1983, **4**, 294–301.

56 R. Krishnan, J. S. Binkley, R. Seeger and J. A. Pople, *J. Chem. Phys.*, 1980, **72**, 650–654.

57 G. D. Purvis and R. J. Bartlett, *J. Chem. Phys.*, 1982, **76**, 1910–1918.

58 G. E. Scuseria, C. L. Janssen and H. F. Schaefer, *J. Chem. Phys.*, 1988, **89**, 7382–7387.

59 H. Koch and P. Jørgensen, *J. Chem. Phys.*, 1990, **93**, 3333–3344.

60 J. F. Stanton and R. J. Bartlett, *J. Chem. Phys.*, 1993, **98**, 7029–7039.

61 Y. Shao, Z. Gan, E. Epifanovsky, A. T. Gilbert, M. Wormit, J. Kussmann, A. W. Lange, A. Behn, J. Deng, X. Feng, D. Ghosh, M. Goldey, P. R. Horn, L. D. Jacobson, I. Kaliman, R. Z. Khaliullin, T. Kuś, A. Landau, J. Liu, E. I. Proynov, Y. M. Rhee, R. M. Richard, M. A. Rohrdanz, R. P. Steele, E. J. Sundstrom, H. L. Woodcock III, P. M. Zimmerman, D. Zuev, B. Albrecht, E. Alguire, B. Austin, G. J. O. Beran, Y. A. Bernard, E. Berquist, K. Brandhorst, K. B. Bravaya, S. T. Brown, D. Casanova, C.-M. Chang, Y. Chen, S. H. Chien, K. D. Closser, D. L. Crittenden, M. Diedenhofen, R. A. DiStasio Jr., H. Do, A. D. Dutoi, R. G. Edgar, S. Fatehi, L. Fusti-Molnar, A. Ghysels, A. Golubeva-Zadorozhnaya, J. Gomes, M. W. Hanson-Heine, P. H. Harbach, A. W. Hauser, E. G. Hohenstein, Z. C. Holden, T.-C. Jagau, H. Ji, B. Kaduk, K. Khistyaev, J. Kim, J. Kim, R. A. King, P. Klunzinger, D. Kosenkov, T. Kowalczyk, C. M. Krauter, K. U. Lao, A. D. Laurent, K. V. Lawler, S. V. Levchenko, C. Y. Lin, F. Liu, E. Livshits, R. C. Lochan, A. Luenser, P. Manohar, S. F. Manzer, S.-P. Mao, N. Mardirossian, A. V. Marenich, S. A. Maurer, N. J. Mayhall, E. Neuscamman, C. M. Oana, R. Olivares-Amaya, D. P. O'Neill, J. A. Parkhill, T. M. Perrine, R. Peverati, A. Prociuk, D. R. Rehn, E. Rosta, N. J. Russ, S. M. Sharada, S. Sharma, D. W. Small, A. Sodt, T. Stein, D. Stück, Y.-C. Su, A. J. Thom, T. Tsuchimochi, V. Vanovschi, L. Vogt, O. Vydrov, T. Wang, M. A. Watson, J. Wenzel, A. White, C. F. Williams, J. Yang, S. Yeganeh, S. R. Yost, Z.-Q. You, I. Y. Zhang, X. Zhang, Y. Zhao, B. R. Brooks, G. K. Chan, D. M. Chipman, C. J. Cramer, W. A. Goddard III, M. S. Gordon, W. J. Hehre, A. Klamt, H. F. Schaefer III, M. W. Schmidt, C. D. Sherrill, D. G. Truhlar, A. Warshel, X. Xu, A. Aspuru-Guzik, R. Baer, A. T. Bell, N. A. Besley, J.-D. Chai, A. Dreuw, B. D. Dunietz, T. R. Furlani, S. R. Gwaltney, C.-P. Hsu, Y. Jung, J. Kong, D. S. Lambrecht, W. Liang, C. Ochsenfeld, V. A. Rassolov, L. V. Slipchenko, J. E. Subotnik, T. V. Voorhis, J. M. Herbert, A. I. Krylov, P. M. Gill and M. Head-Gordon, *Mol. Phys.*, 2015, **113**, 184–215.

62 S. Gozem and A. I. Krylov, *WIREs Computational Molecular Science*, 2022, **12**, e1546.

63 P. Wojcik, S. Gozem, V. Mozhayskiy and A. I. Krylov, *http://iopenshell.usc.edu/downloads*.

64 U. Werner, R. Mitrić, T. Suzuki and V. Bonačić-Koutecký, *Chem. Phys.*, 2008, **349**, 319–324.

65 U. Werner, R. Mitrić and V. Bonačić-Koutecký, *J. Chem. Phys.*, 2010, **132**, 174301.

66 W. C. Swope, H. C. Andersen, P. H. Berens and K. R. Wilson, *J. Chem. Phys.*, 1982, **76**, 637–649.

67 S. Awali, J.-M. Mestdagh, M.-A. Gaveau, M. Briant, B. Soep, V. Mazet and L. Poisson, *J. Phys. Chem. A*, 2021, **125**, 4341–4351.

68 M. A. Kochman, B. Durbeej and A. Kubas, *J. Phys. Chem. A*, 2021, **125**, 8635–8648.